

A Low-Complexity Speech Codec Using Parametric Dithering for ASR

Ellison Murray, Morriel Kasher, and Predrag Spasojevic

Rutgers University

New Brunswick, NJ, USA

{ellison.murray, morriel.kasher}@rutgers.edu, spasojev@winlab.rutgers.edu

Abstract

Dithering is a technique commonly used to improve the perceptual quality of lossy data compression. In this work, we analytically and experimentally justify the use of dithering for ASR input compression. We formalize an understanding of optimal ASR performance under lossy input compression and leverage this to propose a parametric dithering technique for a low-complexity speech compression pipeline. The method performs well at 1-bit resolution, showing a 25% relative CER improvement, while also demonstrating improvements of 32.4% and 33.5% at 2- and 3-bit resolution, respectively, with our second dither choice yielding a reduced data rate. The proposed codec is adaptable to meet performance targets or stay within entropy constraints.

Introduction

Quantization is fundamental to analog-to-digital conversion (ADC) [1] and underlies lossy audio compression methods such as waveform, subband, and transform coding [2, 3]. This process introduces distortion, or quantization error, which can be made less perceptible through dithering.

Dithering extends beyond perceptual coding, having applications in machine learning: federated learning [4] and automatic speech recognition (ASR), and in graphic design (halftoning) [5]. For ASR, frequency-selective dithering has been studied as a means of compensating for the spectral feature distortion of MPEG-3 coding [6].

Previous results have been limited to outdated ASR acoustic models based on Gaussian Mixture Models and early Deep Neural Networks [7], without consideration of critical factors such as implementation complexity and entropy trade-offs. Moreover, there remains a limited rigorous justification for dithering within ASR systems, with primarily black-box evaluations [8] and minimal exploration of its effect on low-level uniform quantization, all of which we aim to address.

Implementation constraints are particularly relevant for enabling real-time offloading of speech data from low-powered wearable electronics [9]. Standard codecs such as Opus provide highly efficient, near-lossless compression even at low rates, but rely on FFT-based computations [10]. A low-complexity speech codec would improve the functionality of speech-interactive wearables, reducing communication barriers for users with hearing impairments or in multilingual environments.

We propose a low-complexity parametric dithering quantization system designed to balance ASR performance and implementation efficiency. We hypothesize a link between ASR accuracy and the total power and the autocorrelation properties of

quantization error. We then introduce two adaptable dither distributions that allow us to explore this trade-off. Through experimental evaluation, we investigate the effectiveness of these distributions and present results that support our framework as a step toward a principled understanding of dithering in ASR.

Background

Dithered Quantizers

We consider a b -bit uniform scalar quantizer with finite resolution ($b \in \{1, 2, 3\}$), operating under a low entropy constraint. While non-uniform quantizers achieve lower distortion at low rates [1], we prioritize the simplicity of uniform quantization for practical implementation. We define this mid-rise quantizer function $Q(\cdot)$ with codebook value output, $C_k = k\Delta + \Delta/2$, and decision boundaries, $T_k = k\Delta$, where $k \in \{1, 2, \dots, 2^b\}$, with k denoting the index of each quantization output bin and Δ denoting size of the bin.

A uniform quantizer, designated as such by $C_{k+1} - C_k = T_{k+1} - T_k = \Delta$, can also operate in a mid-tread configuration ($C_k = k\Delta$, $T_k = k\Delta - \Delta/2$). We adopt the mid-rise configuration, which ensures that the output is centered around zero: a crucial property at low bit depths.

We consider an analog input and dither samples, $x \in X$ and $v \in V$, where X and V are the respective random variables; the quantizer input sample $y \in Y$ is the sum of our input and dither samples $x+v = y$, with random variable Y . The quantizer output is given by $Q(y) \in \{C_1, C_2, \dots, C_{2^b}\}$, where $Q(y) = C_k \implies T_k \leq y \leq T_{k+1}$. The error of our dithered quantization system is computed non-subtractively as $\varepsilon_{\text{NS}} = Q(y) - x$. At low resolution, without dithering, ε_{NS} is strongly correlated with the input signal and time-lagged versions of itself [11], observed by the autocorrelation vector.

The dither V follows the triangular probability density function (TPDF) defined in (1), and is denoted as $f_V(v)$. In the case of no dithering, $f_V(v) = \delta(v)$, while for full dithering $f_V(v) = \Lambda_{2\Delta}(v)$. The input X , corresponding to a speech signal, is approximately modeled as a Laplacian probability distribution [12], $f_X(x) = \frac{1}{2c} \exp(-\frac{|x-\mu|}{c})$ where c is a scale parameter.

$$\Lambda_{2a}(v) \triangleq \begin{cases} \frac{1}{a^2}(a - |v|) & |v| \leq a \\ 0 & \text{otherwise} \end{cases} \quad (1)$$

Though not seen with non-subtractive dithering (NSD), ε_{S} , quantization error under subtractive dithering, achieves full statistical independence from the input signal [13]. Despite this advantage, we neglect the method, as its implementation requires retaining the dither following ADC and results in a high-resolution output [14]; both of which contradict our low-complexity approach. However, under NSD, TPDF dithers ensure that the first and second moments of ε_{NS} are independent from the inputs, where the second moment is minimized [15].

The total error's second moment, also referred to as the Mean Squared Error (MSE), calculated $\mathbb{E}[\varepsilon_{\text{NS}}^2]$, is commonly used as a distortion metric, as it directly

represents the power of the quantization error. With no dithering, $\mathbb{E}[\varepsilon_{\text{NS}}^2] \geq \frac{\Delta^2}{12}$, while with full dithering, $\mathbb{E}[\varepsilon_{\text{NS}}^2] \geq \frac{\Delta^2}{4}$.

ASR Model

OpenAI’s **Whisper** model’s front-end consists of an audio processing block that resamples all input to 16 kHz and computes a mel-spectrogram [16], highlighting the importance of time–frequency analysis for our analysis of speech. The model’s Transformer-based, end-to-end architecture is representative of the dominant frameworks in modern speech recognition [17]; its high out-of-the-box accuracy offers a strong baseline for evaluating the effects of our parameters on a state-of-the-art system.

Analysis

Motivation

Given the reliance of ASR models on feature extraction from log-mel spectrograms and prior work investigating the impact of spectral distortion on ASR performance [16], we consider the structural integrity of Time-Frequency (TF) features “visible” to models as a baseline for optimal dither design. For an error signal ε of total length N with discrete time and frequency indices n and f , we adopt two metrics to characterize this integrity: one quantifies the overall increase in quantization error power (MSE), and the other captures the spectral distribution of the error, both of which are represented by the Power Spectral Density (PSD) as $S_{\varepsilon\varepsilon}(f) = \left| \sum_{n=0}^N \varepsilon(n) e^{-j2\pi f n/N} \right|^2$. We aim for a smooth error power spectrum and minimal frequency energy increase, to best ensure retention of the critical TF patterns that ASR models are trained on.

Taking this into account, we define two independent and identically distributed (iid) dither distributions ($v \sim f_{V_{m,\alpha}}$ (also denoted f_{V_m})) where $V_{m,\alpha}$ is the associated random variable with choice parameter m . The distributions are given by (2). Controlled by the $\alpha \in [0, 1]$ parameter, $f_{V_{1,\alpha}}$ varies only in the proportion of samples allocated to the dither, while $f_{V_{2,\alpha}}$ varies both in the prior sense and with its support interval.

$$f_{V_{m,\alpha}}(v) = \alpha \Lambda_{2\Delta((\alpha-1)m+2-\alpha)}(v) + (1-\alpha)\delta(v) \quad m \in \{1, 2\} \quad (2)$$

There is no difference in the impact parametric dithering has on the PSD of the quantization error signal, $\varepsilon_{m,\alpha}$, across tested bit-depths. As shown in Fig. 1, null dithering concentrates power at 1 kHz, a band critical to speech [18], leading to dominant perceptual distortion. Increasing α progressively shapes the PSD of $\varepsilon_{m,\alpha}$, not only raising the noise-floor power, but also reducing the power around 1 kHz. Across α , the PSD shape evolves non-linearly and uniquely for each dither type, with full dithering yielding a flat error PSD.

For error signal ε , we consider specific sample index n and time-lag τ with which we define autocorrelation vector $r_{\varepsilon\varepsilon}$ where $r_{\varepsilon\varepsilon}(n, \tau) = \mathbb{E}[\varepsilon_n \varepsilon_{n+\tau}]$ s.t. $n, n + \tau \leq N$. Although a speech signal is not strictly WSS, on short time scales, it behaves quasi-WSS [19] so $\forall n, r_{\varepsilon\varepsilon}(\tau) \triangleq r_{\varepsilon\varepsilon}(n, \tau)$. To measure the fine-scale temporal correlations of the quantization error, we propose ACF $_{\tau}$ in (3), where $r_{\varepsilon\varepsilon}(\tau)$ is normalized by

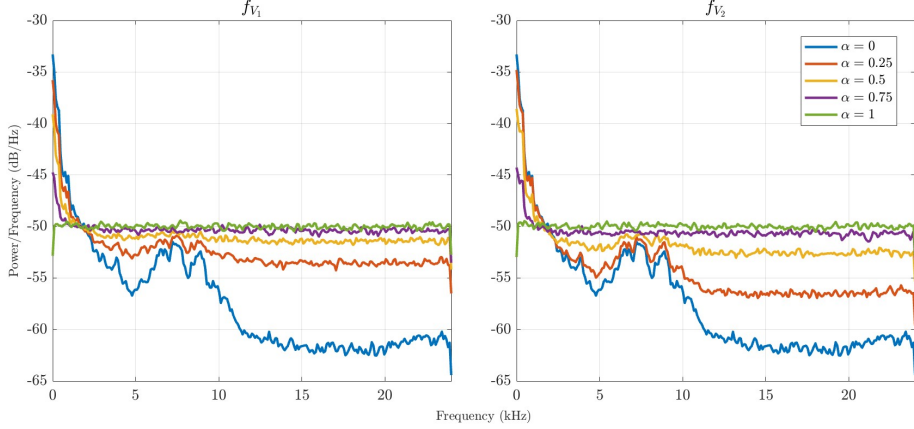


Figure 1: PSD of $\varepsilon_{m,\alpha}$ at 1 Bit for f_{V_1} and f_{V_2} , Given $\alpha = 0, 0.25, 0.5, 0.75$, and 1 , Smoothed With a 480-Sample Window.

$\mathbb{E}[\varepsilon_n^2]$ to remove the scale dependence of the absolute energy of ε . Our choice of $\tau = 5$ reduces sensitivity to purely sample-to-sample artifacts present at $\tau = 1$, yet remains short enough to capture residual correlations, including contributions from both low-frequency energy and high-frequency structures.

$$\text{ACF}_\tau \triangleq r_{\varepsilon\varepsilon}(\tau)/r_{\varepsilon\varepsilon}(0) = \mathbb{E}[\varepsilon_n \varepsilon_{n+\tau}]/\mathbb{E}[\varepsilon_n^2] \quad (3)$$

Increasing α decreases the autocorrelation of the quantization error and increases the total error power, revealing a trade-off between these two metrics and motivating the use of parametric dithering. As shown in Fig. 2, the Pareto front of MSE versus ACF_5 is different between f_{V_1} and f_{V_2} ; however, the trade-off shape is preserved across bit depths, with the curves undergoing a scaling transformation.

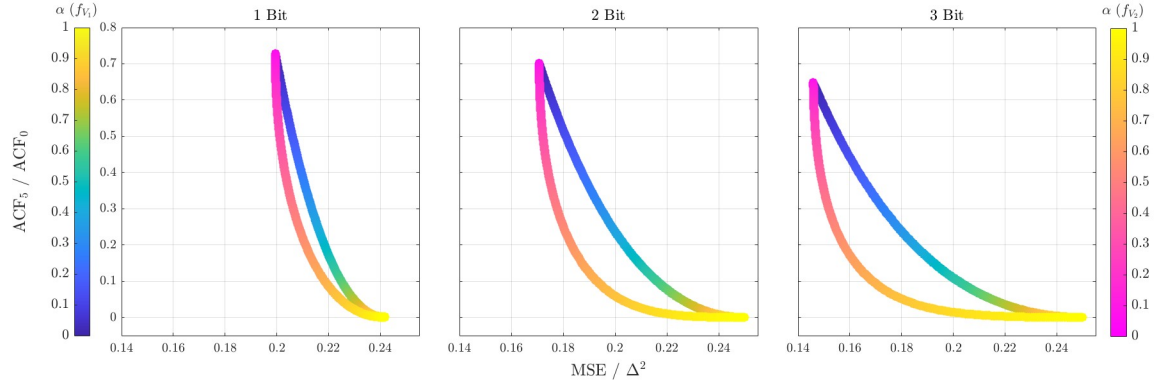


Figure 2: Multi-Objective Performance Comparison between f_{V_1} and f_{V_2} for Tested Bit-Depths

Given this trade-off, we propose that (4) holds as an accurate model for ASR performance, where $M(V_{m,\alpha})$, a weighted combination of MSE and ACF_τ , correlates positively with $P(V_{m,\alpha})$, a direct ASR performance measure based on transcription accuracy, whose observed values vary with α (elaborated further in the

Results section). We use this definition to numerically evaluate the trade-off coefficient, β^* , using (5) over a discretized set of α values, where $\mu_P = \mathbb{E}[P(V_{m,\alpha})]$, $\sigma_P^2 = \mathbb{E}[(P(V_{m,\alpha}) - \mathbb{E}[P(V_{m,\alpha})])^2]$; using equivalent definitions for $M(V_{m,\alpha}, \beta)$.

$$\exists \beta \in [0, 1] \text{ s.t. } \forall \alpha \quad M(V_{m,\alpha}, \beta) = (\beta - 1)\mathbb{E}[\varepsilon_{m,\alpha}^2] + \beta\mathbb{E}[\varepsilon_{m,\alpha_t}\varepsilon_{m,\alpha_{t+\tau}}] \sim P(V_{m,\alpha}) \quad (4)$$

$$\beta^* = \arg \max_{\beta} \frac{\mathbb{E}[(P(V_{m,\alpha}) - \mu_P)(M(V_{m,\alpha}, \beta) - \mu_M)]}{\sigma_P \sigma_M} \quad (5)$$

Rate Computation

In designing an efficient codec, we treat the data rate as a key factor in minimizing the required transmission bandwidth. By (2), α increases entropy, for both f_{V_1} and f_{V_2} . To evaluate the difference between the entropy behaviors of f_{V_1} and f_{V_2} , we consider Shannon's entropy, which represents the theoretical lower bound on the average number of bits per symbol required for lossless compression [20]. Shannon's entropy of output $Q_{m,\alpha}$ can be computed using (6), where $f_{Y_{m,\alpha}}(y) = [f_X(x) * f_{V_{m,\alpha}}(v)](y)$ and $p_k(\alpha) = \int_{T_k}^{T_{k+1}} f_{Y_{m,\alpha}}(y) dy$.

$$H(Q_{m,\alpha}) = - \sum_{k=1}^{2^b} p_k(\alpha) \log_2 p_k(\alpha) \quad (6)$$

While a closed-form expression of Entropy could provide an exact characterization via (6), we gain an intuitive understanding of the dithers' behaviors from our analytical and numerical results.

We begin our analysis by considering the variance of the TPDF dithers as $\sigma_\Lambda^2 \triangleq a^2/4$, from which the variance of $V_{m,\alpha}$ follows: $\sigma_m^2 = \text{Var}(V_{m,\alpha}) \triangleq \frac{\alpha^{2m-1} \Delta^2}{4}$. The variance of a Laplace-distributed speech input is $\text{Var}(X) \triangleq 2c^2$. By principle of our dithers being independent from our input, $\text{Cov}(X, V_{m,\alpha}) = 0$, and therefore, $\text{Var}(X + V_{m,\alpha}) = \text{Var}(X) + \text{Var}(V_{m,\alpha})$. By Sheppard's Corrections analysis, $\text{Var}(Q_{m,\alpha}) \approx \text{Var}(X + V_{m,\alpha}) - \frac{\Delta^2}{12}$ [21]. With this, we apply the Principle of Maximum Entropy, where the Gaussian distribution maximizes entropy for a given variance constraint [22]. For a Gaussian variable Z with variance σ_Z^2 , the differential entropy is $H(Z) = \frac{1}{2} \log_2(2\pi e \sigma_Z^2)$. While (7), which assumes a Gaussian output distribution, does not predict the exact numerical values, it captures the regression for $\alpha \in [0, 1]$ and shows that $H(Q_{1,\alpha}) > H(Q_{2,\alpha})$ in that interval.

$$H(Q_{m,\alpha}) \leq \frac{1}{2} \log_2 \left(2\pi e \left(2c^2 + \sigma_m^2 - \frac{\Delta^2}{12} \right) \right) \quad (7)$$

Fig. 3 numerically validates (7): entropy increases with α , while the trend differs significantly between the two dither types. Entropy for f_{V_1} exhibits a concave shape over alpha, while with f_{V_2} , entropy shows a distinctly convex trend. This convex behavior, a result of the controlled dither support, demonstrates the advantage of f_{V_2} dithering.

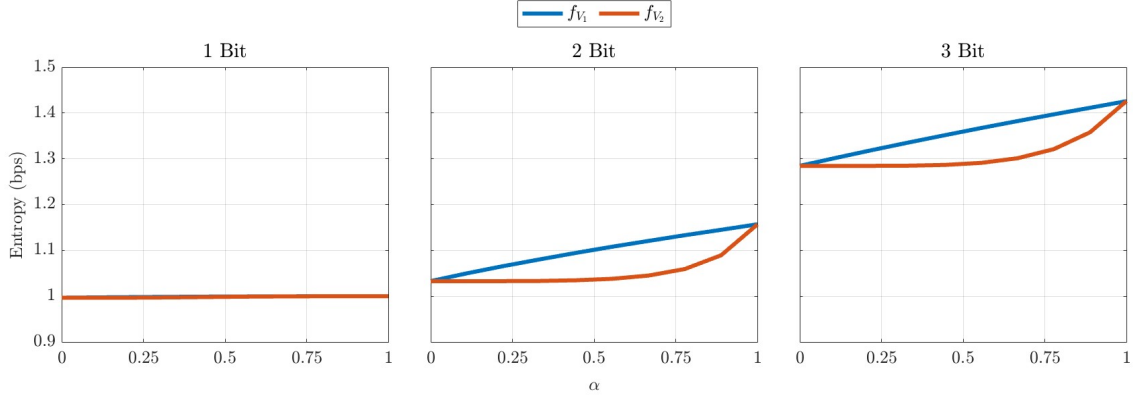


Figure 3: Numerical Results for Shannon's Entropy Over α for Speech Quantized to 1-3 Bits

Codec

The proposed codec follows the pipeline outlined in Fig. 4. Input and dither signals of N samples are summed before being passed through the mid-tread b -bit quantizer. This is followed by Huffman Coding, an optimal lossless compression technique which achieves an average code length within 1 bit of the source entropy.

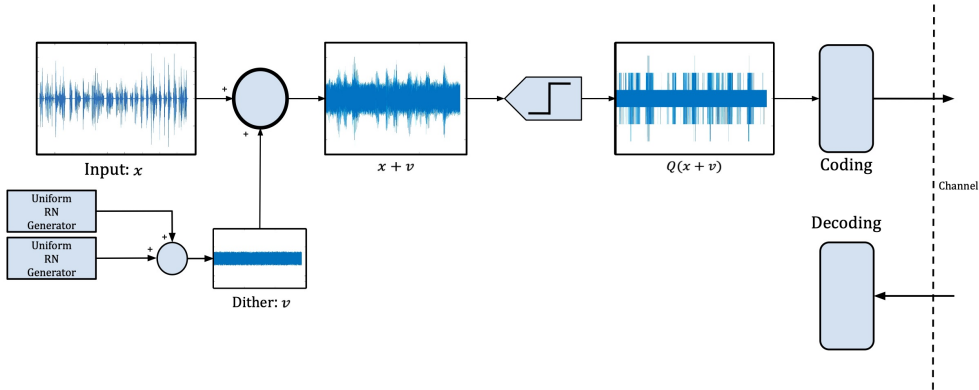


Figure 4: Speech Codec Quantization Pipeline

Results

Experimental Setup

We used 30 identical scripts, distinct voices' speech samples drawn from Google AI's `en-US-Chirp3-HD` voices [23]. All files (16-bit linear PCM, 48 kHz) were imported into MATLAB, where they were amplitude-normalized and trimmed to 20 seconds. Our intelligibility metrics were calculated on the decoded signals, and our rate calculation uses Huffman coding.

We utilize `whisper.cpp`, a high-performance C++ implementation of the original model [24]. Whisper's transcription accuracy is evaluated by the Character Error Rate (CER), computed via the Levenshtein distance. The reference transcript is

taken from the high-quality imported speech itself, rather than a global key, to account for variable content across the clipped samples. The Levenshtein distance is normalized by the reference text length, providing a theoretical score in the range $[0, 1]$, corresponding to $P(V_{m,\alpha}) \triangleq \text{CER}$. To produce a single data point given each bit-resolution and α parameter while accounting for inter-speaker variability, for each metric, we computed the mean and the standard error of the mean (SEM).

ASR Performance

As shown in Fig. 5, $P(V_{m,\alpha})$ is minimized by parametric dithering for all tests. Despite the lower overall $P(V_{m,\alpha})$ at 3-bit resolution (maximum absolute improvement = 0.0271), the largest absolute gains occur at 1- and 2-bit quantization (0.0449 and 0.0486 improvement), suggesting weaker motivation at the higher resolution case.

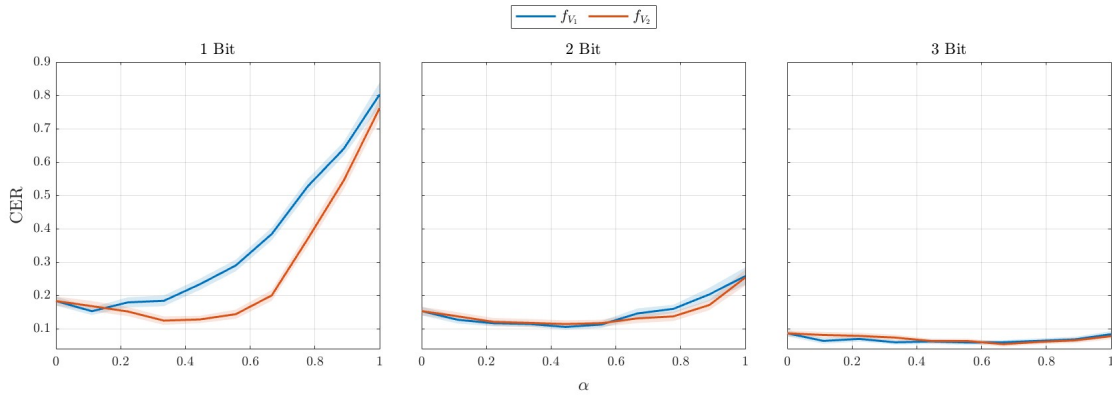


Figure 5: $P(V_{1,\alpha})$ and $P(V_{2,\alpha})$ Results Across α ; Shaded Regions Indicate the SEM

Model Verification

The verification of metric $M(V_{m,\alpha})$ is verified using the method prescribed by (4). The β^* that satisfy the model are shown in Table 1, where β^* is shown to vary across bit-depth, and less significantly between the two dither types. Total power of ε_{NS} (MSE) holds a substantially larger weight in $M(V_{m,\alpha})$ than the shape of noise floor (ACF₅); both qualities are relevant. Notably, ACF₅ holds more weight at higher rates. Fig. 6 visualizes the fit of $M(V_{m,\alpha})$ to the results of $P(V_{m,\alpha})$.

Table 1: Computed β^* Values

Bit-Depth	1	2	3
f_{V_1}	0.0303	0.0808	0.141
f_{V_2}	0.0303	0.0505	0.152

Optimal Alpha

The optimal α value, α^* , is determined by evaluating both CER improvement and rate. However, for 1-bit quantization, the entropy remains constant, making CER

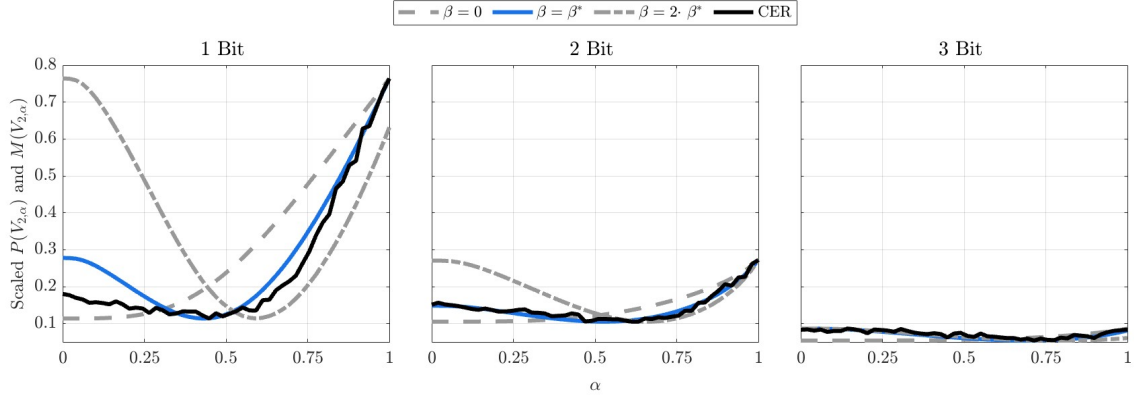


Figure 6: Scaled $M(V_{2,\alpha})$ Within the Range of $P(V_{2,\alpha})$ and Fitted to $P(V_{2,\alpha})$ for β^* and Local β Values.

the sole determining factor for optimization. The α^* computed by (8), where $R(\alpha)$ denotes the rate (Huffman coding) given α and $P(\alpha) = P(V_{m,\alpha}(\alpha))$, are shown in Fig. 7. The α^* for f_{V_2} is consistently larger than that of f_{V_1} even at similar CER improvement, reflecting the reduced rate inherent to f_{V_2} .

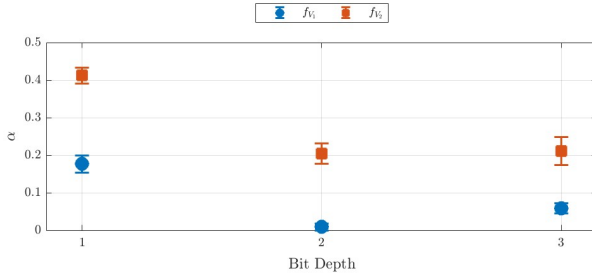


Figure 7: Computed α^* Values with SEM Error Bars

$$\alpha^* = \arg \max_{\alpha: P(\alpha) < P(0)} \frac{P(0) - P(\alpha)}{R(0) - R(\alpha)} \quad (8)$$

Rate Distortion

Fig. 8 shows that at 1-bit quantization, $f_{V_2}(\alpha^*)$ dithering yields a lower CER than $f_{V_1}(\alpha^*)$, showing clear dominance under the most extreme entropy constraint. While increasing the quantization resolution improves ASR performance, it also raises the data rate and provides diminishing returns in CER improvement. As the rate continues to increase, $f_{V_1}(\alpha^*)$ dithering eventually matches and slightly surpasses $f_{V_2}(\alpha^*)$, until their performances become indistinguishable. Notably, at 1-bit quantization, $f_{V_2}(\alpha^*)$ is most justified: not only outperforming null and full dithering by a significant margin, but also achieving minimal rate.

Conclusion

We propose a low-complexity, entropy-constrained speech compression codec design optimized for ASR. We introduced a framework for characterizing ASR performance

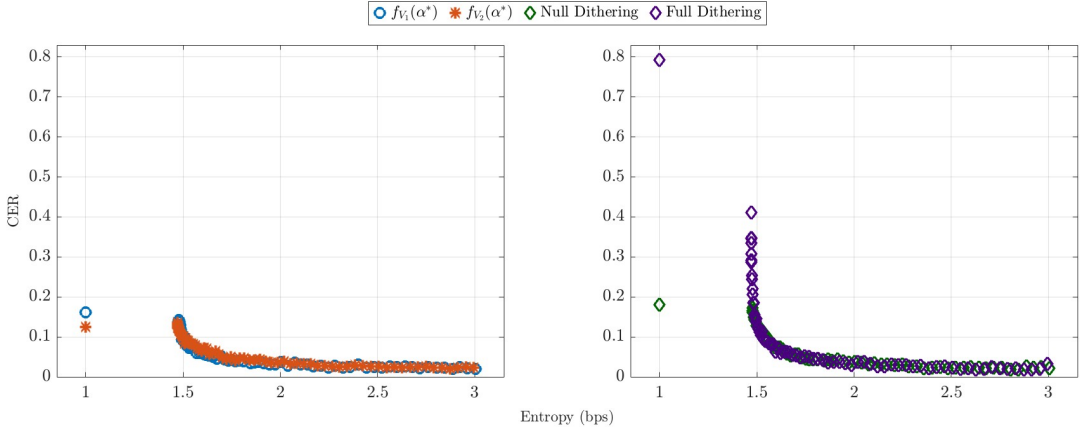


Figure 8: (a) CER of $f_{V_1}(\alpha^*)$ and $f_{V_2}(\alpha^*)$ Dithering Compared to (b) CER of Null and Full Dithering as a Function of Entropy

using MSE and ACF_5 , providing a quantitative basis for designing and evaluating dithering strategies. Our experiments demonstrate the effectiveness of 1-bit quantization with parametric dithering, achieving a critically low CER and yielding a 25% relative improvement compared to null-dithering. These results highlight the potential of ultra-low bit-depth quantization as a viable approach for speech waveform coding in resource-constrained systems.

Future directions include retraining a transformer-based encoder-decoder ASR model to evaluate the limits of parametric dithering more fully. Additional work may focus on expanding the ASR performance model through broader testing and consideration of supplementary objective measures, further validating the role of dithering in ultra-low-resolution speech coding.

References

- [1] R. M. Gray and D. L. Neuhoff, “Quantization,” *IEEE Transactions on Information Theory*, vol. 44, no. 6, pp. 2325–2383, Oct. 1998.
- [2] J. Vanderkooy and S. P. Lipshitz, “Dither in digital audio,” 1987, [Online]. Available: <https://aes2.org/publications/elibrary-page/?id=5173>.
- [3] K. Brandenburg, “MP3 and AAC EXPLAINED,” Tech. Rep., Fraunhofer Institute for Integrated Circuits, Erlangen, Germany, n.d.
- [4] S. K. Lo, Q. Lu, L. Zhu, H. y. Paik, X. Xu, and C. Wang, “Architectural patterns for the design of federated learning systems,” *Journal of Systems and Software*, 2021, Special issue on Software Architecture and Artificial Intelligence.
- [5] P. Freitas, M. Farias, and A. Araujo, “Fast inverse halftoning algorithm for ordered dithered images,” in *2011 24th SIBGRAPI Conference on Graphics, Patterns and Images*, Alagoas, Brazil, 2011, pp. 250–257.
- [6] Michal Borsky, Petr Mizera, and Petr Pollak, “Spectrally selective dithering for distorted speech recognition,” in *InterSpeech*, 2015, Emails: borskmic@fel.cvut.cz, miz-erpet@fel.cvut.cz, pollak@fel.cvut.cz.
- [7] Michal Borsky, Petr Mizera, Petr Pollak, and Jan Nouza, “Dithering techniques in automatic recognition of speech corrupted by mp3 compression: Analysis, solutions and experiments,” *Speech Communication*, vol. 86, pp. 75–84, 2017.

- [8] M. Borsky, P. Pollak, and P. Mizera, “Advanced acoustic modelling techniques in mp3 speech recognition,” *EURASIP Journal on Audio, Speech, and Music Processing*, vol. 2015, no. 1, pp. 20, 2015.
- [9] K. Ha, Z. Chen, W. Hu, W. Richter, P. Pillai, and M. Satyanarayanan, “Towards wearable cognitive assistance,” Tech. Rep. CMU-CS-13-134, Sch. of Comput. Sci., Carnegie Mellon Univ., Pittsburgh, PA, Dec. 2013.
- [10] K. Vos, K. V. Sørensen, S. S. Jensen, and J.-M. Valin, “The opus codec,” in *135th AES Convention*, New York, USA, 2013.
- [11] R. M. Gray and T. G. Stockham, “Dithered quantizers,” *IEEE Transactions on Information Theory*, vol. 39, no. 3, pp. 805–812, May 1993.
- [12] S. Gazor and Wei Zhang, “Speech probability distribution,” *IEEE Signal Processing Letters*, vol. 10, no. 7, pp. 204–207, July 2003.
- [13] Stanley P. Lipshitz, Robert A. Wannamaker, and John Vanderkooy, “Quantization and dither: A theoretical survey,” *Journal of the Audio Engineering Society*, vol. 40, no. 5, pp. 355–375, 1992.
- [14] Morriel Kasher, Michael Tinston, and Predrag Spasojevic, “Distortion-Controlled Dithering with Reduced Recompression Rate,” *arXiv e-prints*, feb 2024.
- [15] Robert A. Wannamaker, Stanley P. Lipshitz, John Vanderkooy, and J. Nelson Wright, “A theory of non-subtractive dither,” *Journal of the Audio Engineering Society*, vol. 40, no. 7/8, pp. 571–583, 1992.
- [16] Alec Radford, Jong Wook Kim, Tao Xu, Greg Brockman, Christine McLeavey, and Ilya Sutskever, “Robust speech recognition via large-scale weak supervision,” *arXiv preprint arXiv:2212.04356*, 2022.
- [17] M. Božić and M. Horvat, “A survey of deep learning audio generation methods,” *arXiv preprint*, 2024, arXiv:2405.20146. [Online].
- [18] T. Ikuma, A. J. McWhorter, E. Oral, and M. Kunduk, “Formant-aware spectral analysis of sustained vowels of pathological breathy voice,” *Journal of Voice*, 2023.
- [19] Wing-Kin Ma, Tsung-Han Hsieh, and Chong-Yung Chi, “Doa estimation of quasistationary signals with less sensors than sources and unknown spatial noise covariance: A khatri-rao subspace approach,” *IEEE Transactions on Signal Processing*, vol. 58, no. 4, pp. 2168–2180, April 2010.
- [20] S. R. Kulkarni, “Ele 201: Information signals - course notes, chapter 8: Information, entropy, and coding,” 2014.
- [21] S. B. Vardeman, “Sheppard’s correction for variances and the ”quantization noise model”,” *IEEE Transactions on Instrumentation and Measurement*, vol. 54, no. 5, pp. 2117–2119, Oct 2005.
- [22] Keith Conrad, “Probability distributions and maximum entropy,” Expository papers, n.d., Accessed on 2025-08-22.
- [23] GoogleCloudPlatform, “get_started_with_chirp_3_hd.voices.ipynb – Generative AI Audio Example,” GitHub repository, 2025, [Online]. Available: https://github.com/GoogleCloudPlatform/generative-ai/blob/main/audio/speech/getting-started/get_started_with_chirp_3_hd.voices.ipynb [Accessed: Sep. 24, 2025].
- [24] ggml-org, “whisper.cpp: A high-performance, dependency-free port of OpenAI’s Whisper model,” GitHub repository, 2025, [Online]. Available: <https://github.com/ggml-org/whisper.cpp> [Accessed: Sep. 24, 2025].